CHAPTER V

RESULTS AND DISCUSSIONS

V-1. Thermodynamic Study.

Chemical thermodynamics is always the prerequisite for a study of any chemical reaction. This is because that it not only can supply valuable information about energetic properties of the reacting system, but also can provide data of equilibrium conditions as standard reference for evaluating the actual performance of the reaction system. The primary goal of the thermodynamic study in this research was to obtain the equilibrium enthalpy change of the reaction to be utilized in the evaluation of the intraparticle temperature gradient.

Equilibrium molar rates of chemical species present in the reacting system at specific reaction conditions were first determined by a scheme developed by Balzhiser et al. [13]. In this method, an alternative linear system of algebraic equations derived from the problem to minimize the total Gibbs free energy for the reacting system, is solved. Details of the methodology are given in Appendix L. Multiplying the difference, in molar rate, of each individual species between feed and

equilibrium product by its corresponding heat of formation at a specified temperature yields the enthalpy change for this particular species. The sum of all individual enthalpy changes gives the net equilibrium enthalpy change of the reaction. A computer software program THERMODY was coded to actually execute all the computations and is listed in Figure K.1 in Appendix K. Thermodynamic data for individual chemical species were obtained from the thermodynamic tables compiled by API [207]. The initial guesses of equilibrium molar rates and feed molar rates for all simulations were taken from steady state experiments.

Equilibrium enthalpy changes of nine simulations (I through IX) of different sets of chemical species were obtained and are summarized in Table 5.1 along with the Gibbs free energy change and equilibrium constant. Input data and resulting equilibrium molar rates of all species are listed in Tables L.1 through L.9 of Appendix L. All the changes of equilibrium enthalpy and Gibbs free energy were negative which agreed with the calculations of conventional Fischer-Tropsch synthesis, although most of them were less exothermic. The modified Fischer-Tropsch reaction is more thermodynamically favorable than its conventional competitor.

Additional equilibrium data, percentage conversions of

Table 5.1. Equilibrium Thermodynamic Properties for the MFTR System Obtained by the Thermodynamics Studies I through IX.

Simulation Study	Reaction Temperature (°K)	Enthalpy Change (cal.)	Gibbs Free Energy Change (cal.)	Equilibrium Constant
I	483.15	-1,897.9990	-1,082.0732	3.0868
II	494.26	-19,863.0234	-12,615.6992	3.7916×10^{5}
III	494.26	-7,016.3242	-4,615.3437	1.0989×10^{2}
IV	494.26	-6,996.3320	-4,634.7148	1.1208×10^{2}
V	522.04	-1,910.7544	-819.2952	2.2030
VI	531.48	-4,998.4102	-2,036.9978	6.8818
VII	555.37	-26,402.1875	-17,960.0078	1.1701×10^{7}
VIII	563.71	-3,071.6851	-2,262.4346	7.5373
IX	594.26	-3,071.4932	-2,219.0464	6.5488

the five active components, namely hydrogen, carbon monoxide, ethylene, carbon dioxide and methane, were also calculated and are listed in Table 5.2 to serve as an upper limit bound that the reaction could proceed at the specified conditions. Hydrogen is almost completely consumed. The conversion of carbon monoxide is hindered by ethylene incorporation. At higher temperatures, e.g., above 550 °K, carbon monoxide is generated rather than consumed. Carbon dioxide, on the contrary, is consumed instead of produced. Methane is always generated in large amounts. In general, the presence of olefins in the product lowers the Gibbs free energy change, thus stabilizing the product.

It was also interesting to see how the variation of reaction temperature could affect the equilibrium of a given reaction system. Thus, different types of simulations (X and XI) were performed for the same set of 70 components but utilizing different input compositions. The component molar flow rates of hydrogen, carbon monoxide, ethylene, carbon dioxide and methane in the feed of simulation study X were 28.27, 17.54, 23.99, 9.32 and 4.99 gm-moles/hr respectively. For simulation study XI, the rates of hydrogen and methane were changed to 33.98 and 4.05 gm-moles/hr. The other three components were not varied. The initial and final equilibrium molar rates of all components of both simulations are given in

Table 5.2. Equilibrium Percentage Conversions of Active Species by Thermodynamics Studies I through IX.

Simulation Study	Number of Components	Equilibrium Percentage Conversions (%)					Iterations to converge
		Hydrogen	Carbon Monoxide	Ethylene	Carbon Dioxide	Methane	
I	32	99.9966	95.9585	99.9999	-38.4258	-167.9570	91
II	67	99.9998	73.9743	99.9944	-67.6952	-412.2375	30
III	59	99.9999	6.8432	99.7866	-6.0982	-147.1182	15
IV	76	99.9999	5.9345	99.7874	-5.3634	-148.4409	21
V	42	99.9999	83.4649	99.9595	-37.6465	-86.3701	65
VI	45	99.9998	68.3438	99.9105	-64.7268	-90.1627	27
VII	39	99.9955	-5.9990	99.9437	5.4471	-159.1114	18
VIII	51	99.9948	-23.3606	99.9219	22.2562	-218.7014	34
IX	72	99.9831	-23.8068	99.9416	22.7714	-220.0639	42

Tables L.10 and L.11 of Appendix L.

Equilibrium conversions obtained by the studies X and XI are summarized in Tables 5.3 and 5.4. It can be seen that the equilibrium percentage conversions of all three active reactants, i.e., hydrogen, carbon monoxide and ethylene, generally decline as the reaction temperature increases, which is in accordance with the principle of LeChatelier and Braun. Ethylene is almost completely consumed below 600 °K. Above 700 °K, carbon monoxide is again generated instead of consumed. This implies that totally different types of reactions may occur. The simulation failed to converge for most temperatures below 400 °K; however, maximum conversions, i.e., 100%, for all three active reactants were unexpectedly obtained at the temperature of 250 °K by the simulation.

Usually a decrease in number of moles is involved in the synthesis reactions. Therefore, the equilibrium conversion should increase with increasing operating pressure. At moderate to high pressures, large conversion may be obtained even with positive change of Gibbs free energy. A variety of molecules of different types, carbon numbers and carbon chain structures can be produced by the synthesis reaction up to 500 °K, particularly at elevated pressures, and the distribution of molecules depends on the selectivity of the catalyst

Table 5.3. Temperature Effect on the Equilibrium Percentage Conversions of Active Species by Thermodynamics Study X.

Temperature (°K)	Equilibrium Percentage Conversions (%)					Iterations to converge
	Hydrogen	Carbon Monoxide	Ethylene	Carbon Dioxide	Methane	
250.0	100.0000	100.0000	100.0000	-94.1626	-586.5208	25
450.0	99.5032	99.8763	100.0000	-78.0168	-809.1672	105
533.2	90.3409	98.4645	100.0000	-68.8315	-769.4880	140
573.2	91.2258	88.8828	100.0000	-70.0344	-722.4856	147
600.0	75.4384	86.8331	100.0000	-62.9771	-671.4744	815
650.0	65.5388	44.1041	99.9999	-23.0858	-719.3625	532
750.0	97.0823	-57.4455	99.9908	54.1966	-720.0774	26
900.0	82.1652	-103.5697	99.9227	97.5584	-690.7534	25
950.0	73.0665	-105.1999	99.8543	99.0742	-657.0259	28
1000.0	61.5076	-105.7972	99.7408	99.6232	-613.2903	30

Table 5.4. Temperature Effect on the Equilibrium Percentage Conversions of Active Species by Thermodynamics Study XI.

Temperature (°K)	Equilibrium Percentage Conversions (%)					Iterations to converge
	Hydrogen	Carbon Monoxide	Ethylene	Carbon Dioxide	Methane	
250.0	100.00	100.00	100.00	-94.1704	-825.4976	25
450.0	99.8690	99.7109	100.00	-78.3261	-1063.2583	147
500.0	96.96	99.46	100.00			134
518.2	92.96	99.31	100.00			336
523.2	92.2061	99.2216	100.00	-63.4907	-1032.2856	418
550.0	91.7410	96.6368	100.00	-73.1398	-998.7710	180
553.2	98.0859	88.1769	99.9999	-71.4626	-981.4021	253
573.2	91.45	90.85	100.00			119
600.0	91.6496	75.7485	99.9999	-59.2295	-969.4070	721
650.0	99.5590	43.6502	99.9987	-40.9952	-917.1677	36
700.0	31.3089	-21.6763	99.9999	37.6709	-808.9902	152
800.0	93.8159	-80.6188	99.9848	76.0660	-975.7988	28
1000.0	64.4373	-105.7582	99.7569	99.5894	-829.0823	30

used. The most negative free energy change is associated with methane formation which means that methane can be the predominant product if it is included as a product species.

For a given catalyst, the product distribution will be shifted by changing the temperature in the direction indicated by the Gibbs free energy change. The product spectrum is also a complex function of feed composition. The reaction thermodynamics and the thermodynamics of interfacial phenomena have not been well studied for the Fischer-Tropsch and related syntheses. The latter can be useful in providing additional clues to the possible surface intermediates in the reaction path [64].

V-2. Catalyst Characterization.

This part of experimental work was not directly related to the kinetic modelling. The objective was two-fold: one was to specify the catalyst used, and the other was to develop a more proper means of defining the activity of the catalyst in terms of the number of active sites of the catalyst. The first goal was achieved through the experiments of XRD (including both powder diffraction and line broadening) and XRF. The latter should be the essence of precise rate representation for heterogeneous catalytic reaction and was accomplished by chemisorption experiments.

A typical X-ray diffraction pattern of the catalyst sample before reduction obtained by the diffractometer is shown in Figure E.1(a) of Appendix E. A reference catalyst of Baker cobalt oxide and MCB activated alumina was also analyzed by the XRD and is presented in Figure E.1(b). Comparing the intensity ratio with the JCPDS' standard pattern of #9-418 (see Figure E.2 in Appendix E), the identification of Co_3O_4 structure was obvious. After reduction or reaction, the pattern became so detoured that the structure of Co_3O_4 was no longer identifiable. ALCOA F-1 activated alumina was not identified simply due to lack of an appropriate standard pattern.

The bulk concentration of cobalt in the catalyst was determined by the X-ray florescence spectrometer. The results are shown in Table F.2 of Appendix F. All catalysts were from the same batch, but screened according to different mesh sizes. For catalyst samples either larger than 60 mesh or smaller than 200 mesh, the bulk content of cobalt were slightly higher than in between these two sizes. This can be attributed to the fact that the larger alumina particles have more pores into which cobalt molecules can diffuse. The adherence of cobalt to the alumina in impregnated catalyst normally is not very strong, and vigorous shaking of the catalyst can either allow more cobalt particles to deeply penetrate the pores of the support, or separate the cobalt particles from the support. Also, the cobalt particles are much smaller than alumina and they are in the form of clusters.

The 311 peak width at $\theta = 36.83°$ of the X-ray diffraction pattern of the cobalt catalyst was compared with the 311 peak width of ALCOA F-1 activated alumina at 38.2° (see Figures E.3(a) and E.3(b) in Appendix E). The difference was used to calculate mean crystallite size of the catalyst of 198.49 Å. The details of calculation are given in Appendix E. The surface area was estimated to be 181.36 m^2/g for either cubic or spherical crystallite [128]. The value of surface area

obtained seems to be too high according to Zowitlak and Bartholomew [250] and possibly attributable to instrument or standard limitations.

Selective hydrogen adsorption measured 5.29×10^{19} active sites per gram of catalyst and about 3.62 m^2/g of cobalt surface area of fresh catalyst after reduction. Sample calculations of initial number of active sites and the cobalt surface area are given in Appendix D. The computation was done based on two assumptions: the stoichiometric coefficient was 1.0 hydrogen atom per surface atom of cobalt, and the site density was 14.6 active sites per square nanometer. Both values were taken from the literature [181]. A typical setup of the chemisorption experiment is shown in Table D.1 of Appendix D. Complete reduction of cobalt/alumina catalyst is difficult, but 30-40% of reduction can be easily achieved in two hours [50].

The stability of the catalyst activity was checked by extended long runs under steady state conditions at the chosen base point specified in Table 5.5. A typical result for reactant conversion versus on-stream time for such an experiment is shown in Figure 5.1. In general, with well-controlled operating conditions, steady state could be reached in 2-3 hours for a fresh catalyst and the catalyst seemed to have a rather long life, say at

Table 5.5. Experimental Conditions - Base Point.

Catalyst: cobalt oxide (in the form of Co_3O_4) supported by ALCOA F-1 activated alumina (60 - 150 mesh).

Mean catalyst crystallite size: 198.49 Å by XRD line broadening.

Bulk cobalt content: 9.3 wt.% by XRF.

Number of initial active sites of the fresh catalyst after reduction: 5.29×10^{19} cobalt atoms per gram of catalyst by volumetric chemisorption.

Specific surface area: 3.62 m^2/gm of catalyst by volumetric chemisorption.

Operating temperature: 494.3 °K.

Operating pressure: 140 psig.

Component molar flow rates in feed, gm-mol/hr:

hydrogen - 0.5355,

carbon monoxide - 0.6664,

ethylene - 0.2676,

carbon dioxide - 0.6946,

methane - 0.3871.

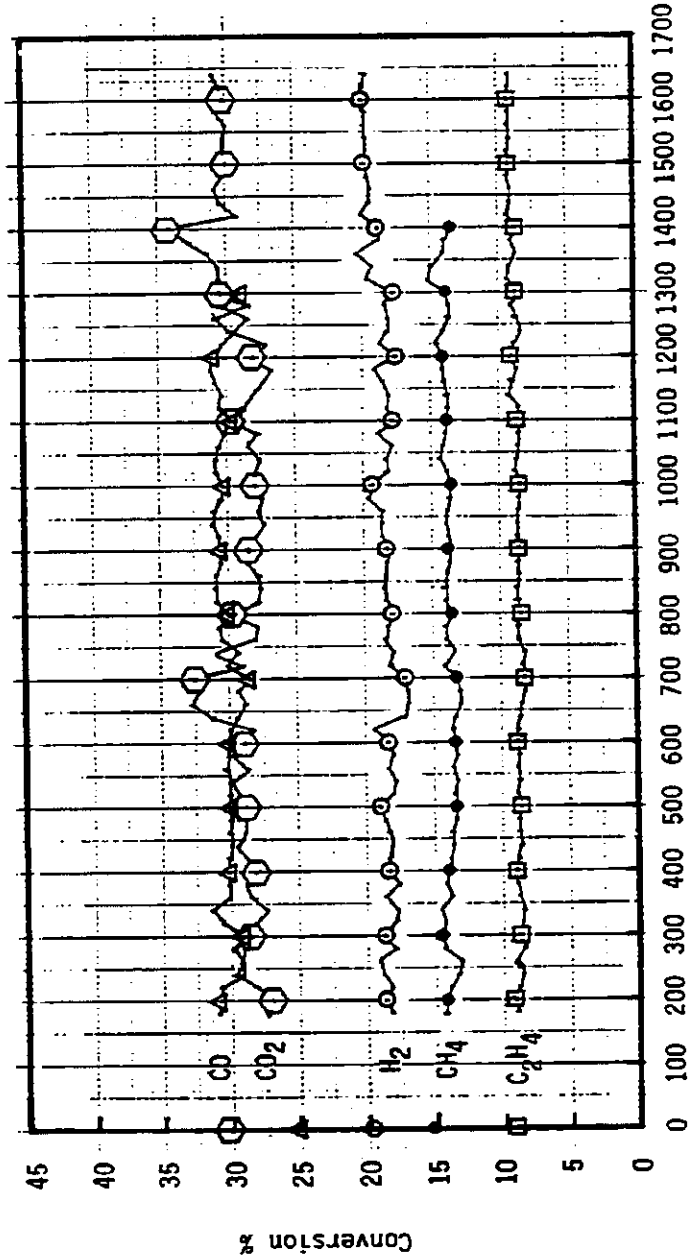

Figure 5.1. Reactant Conversions of an Extended Experiment.

least about a week. Deactivation of the catalyst under the differential mode of operation appears not to be significant for the run times utilized in the experiments.

Catalyst preparation is responsible for the activity condition of the catalyst, but catalyst characterization provides a means to specify the catalyst. It is the ultimate goal of catalysis research that the characteristics of a catalyst can be be correlated to the performance of its function in the catalyzed reaction and, hence, a desirable catalyst can be designed and manufactured for any catalytic reaction. At present, catalysis research has been progressing with the rapid advances in surface science, yet the goal of a priori design of catalysts is still far from being realized.

V-3. Justification for Kinetic Experiments.

The goal of this phase of the experimental work was to determine a reaction regime where the physical transport steps are not the dominating factors and to minimize their effects so that the intrinsic rate of the surface reaction can be observed. The safety reaction regime is interpreted in terms of the appropriate operating conditions for the legitimate kinetic experiments. The justification was accomplished via both experiments and theoretical calculations. The latter relies heavily on the availability and accuracy of various transport parameters, while the experimental method can be very reliable and efficient.

Following the strategy in Figure 4.8, the net reaction rate over a heterogeneous porous catalyst were varied by the change of the operating temperature. The experimental conditions for the temperature effect study are summarized in Table 5.6. The intrinsic rate can only be observed when the operating temperature approaches the lower bound where the reaction proceeds on the catalyst surface so slowly that it governs the process. At higher temperatures, the reaction proceeds faster than the mass transfer steps. Then, either internal diffusion or external diffusion may dominate the net rate of the process, and consequently, the observed rate no longer

Table 5.6. Experimental Conditions - Temperature Studies.

Run	Catalyst		Operating Pressure (psig)	Components in Feed (millipounds per hour)				
	Loading (gm)	Particle Size (meshes)		Hydrogen	Carbon Monoxide	Ethylene	Carbon Dioxide	Methane
1	1.0	60-150	140	2.38	41.15	16.55	67.39	13.69
2	1.0	60-150	140	0.57	8.09	4.99	6.70	2.30
3	1.5	60-150	140	2.36	32.00	17.60	27.60	12.00
4	1.0	60-150	140	2.98	51.44	28.97	67.39	13.69

represents the true reaction rate [238].

This phenomenon has been emphasized by Satterfield and Cortez [190] and is also observed in the justification experiments (see Figure 5.2). It is obvious that there is a turning point in the temperature range between 530 and 550 °K, above which the net rate becomes less dependent on temperature. Further evidence can be seen by temperature studies 2 and 3 (Figure 5.3). Apparently, external diffusion could control the overall rate above 540 °K. One way to reduce the resistance to the external mass transfer is to run the experiment below this temperature.

Hulburt and Srini Vasan suggested that it is necessary to change mass velocity and bed volume in proportion to maintain constant residence time, for the test of the presence of an external diffusion gradient in a packed bed [120]. The experimental conditions for diffusion effect study are given in Table 5.7. Notice that, in Table 5.7, the component mass flow rates in the feed for diffusion studies 5 through 9 represent the base conditions. Figure 5.4 suggests that external diffusion resistance may be minimized for the experiments using the catalysts of 60-150 mesh sizes at the reaction temperature of 494.3 °K if the mass velocity of the feed exceeds 400 gms/cm-hr. Using two different bed depths

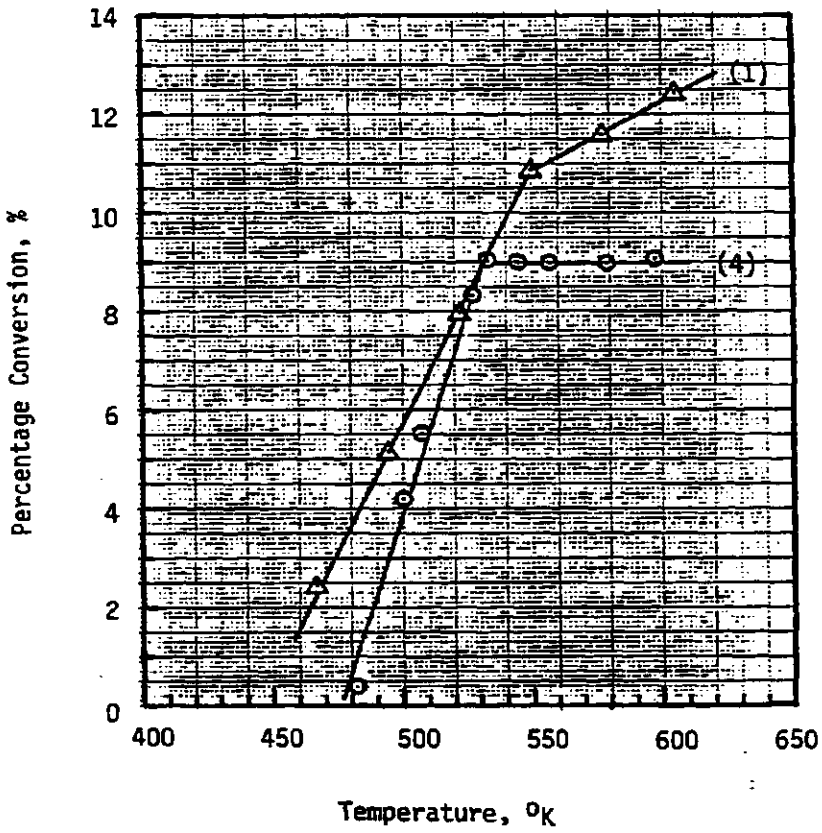

Figure 5.2. Temperature Effect on Reactant Conversion.

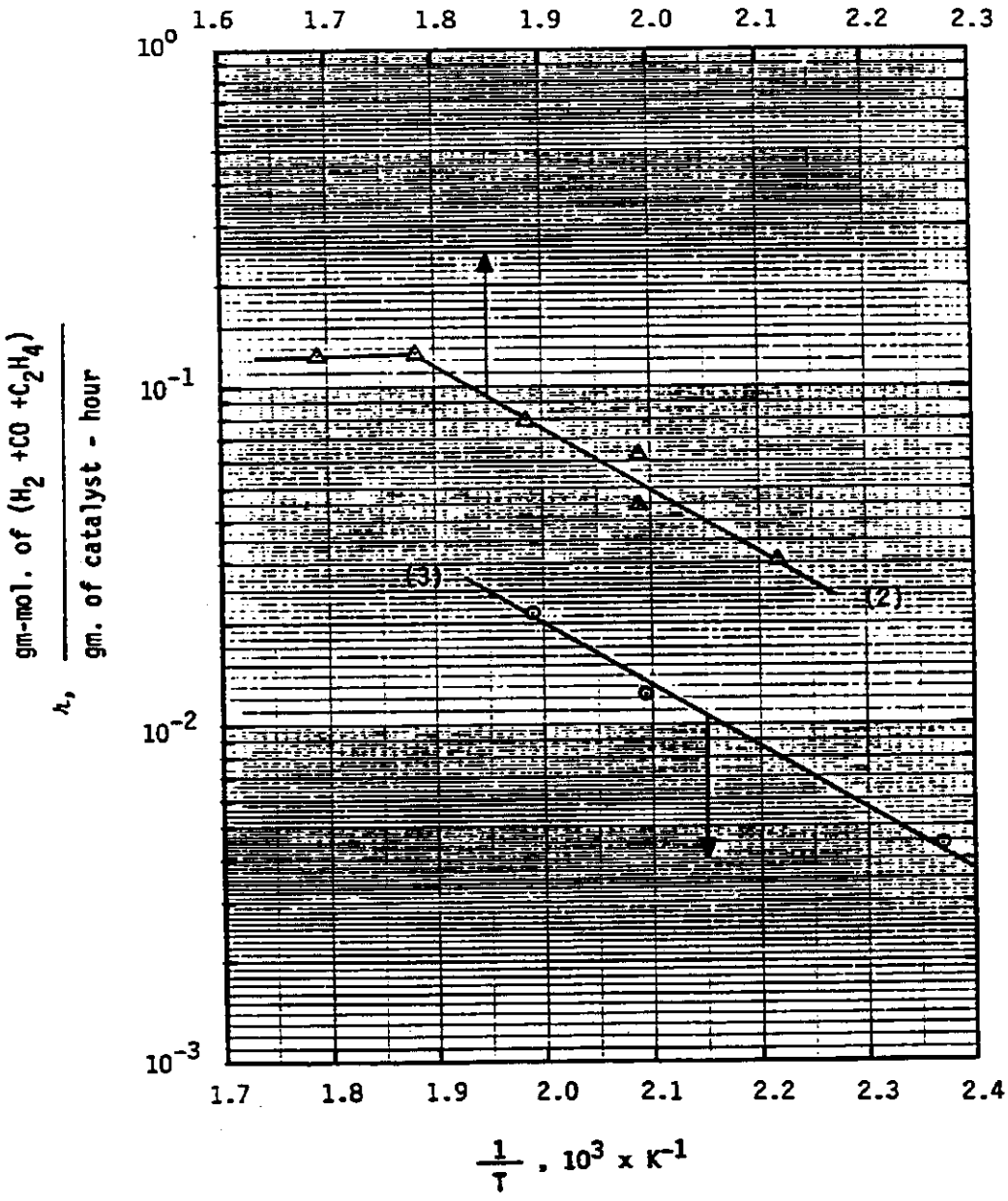

Figure 5.3. Temperature Effect on Reaction Rate.

Table 5.7. Experimental Conditions - Diffusion Studies.

Run	Catalyst		Operating Temperature (°K)	Operating Pressure (psig)	Components in Feed (millipounds per hour)				
	Loading (gm)	Particle Size (meshes)			Hydrogen	Carbon Monoxide	Ethylene	Carbon Dioxide	Methane
1	1.50	60-150	494.3	140	1.18	16.0	8.8	13.8	4.2
2	3.12	60-150	494.3	140	2.36	32.0	17.6	27.6	12.0
3	4.68	60-150	494.3	140	3.54	48.0	26.4	41.4	18.0
4	6.25	60-150	494.3	140	4.72	64.0	35.2	55.2	24.0
5	1.00	60-150	494.3	140	1.18	16.0	8.8	13.8	0.0
6	1.00	60-150	555.4	140	1.18	16.0	8.8	13.8	0.0
7	1.00	>60	494.3	140	1.18	16.0	8.8	13.8	4.2
8	1.50	<150	494.3	140	1.18	16.0	8.8	13.8	4.2
9	1.50	<150	555.4	140	1.18	16.0	8.8	13.8	4.2

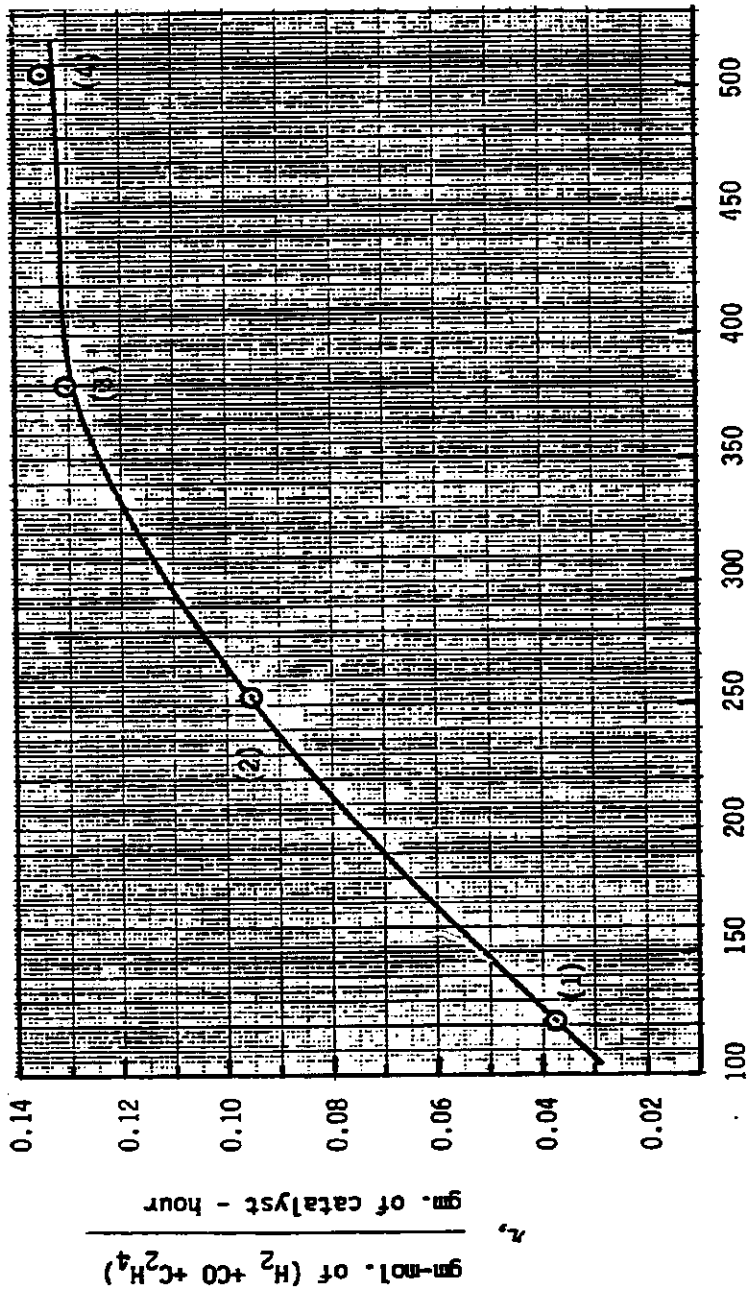

Figure 5.4. Effect of Feed Mass Velocity on Reaction Rate.

of catalyst and three catalyst sizes, the variation of reactant conversion with respect to the change of mass velocity makes it possible to test for both film- and pore-diffusion gradients [73]. The results of this type of testing are plotted in Figures 5.5 and 5.6. It is seen that the conversions of three different particle size experiments coincide when $W/\Sigma F_i$ is less than 0.55 gm of catalyst/gm.mol-hr at low reaction temperature. This means that the external diffusion effect can be minimized when the reaction is operated with $W/\Sigma F_i$ smaller than this value at low temperature for the sizes of catalyst particles chosen. When the catalyst particle is crushed to reduce the size to smaller than 60 mesh, neither the external nor the internal mass transfer will be the controlling factor.

The results of a carefully performed temperature study are plotted in an Arrhenius-type diagram (Figure 5.7). It becomes clear that minimum effects of both external and internal diffusions can be secured under the following operating conditions: (1) reaction temperature is less than 498 °K, (2) weight hourly space velocity (WHSV) is greater than 41.4 gm/hr of feed per gram of catalyst, and (3) the catalyst particle size is smaller than 60 mesh for this modified Fischer-Tropsch reaction to be examined kinetically. The corresponding net activation energy was also estimated to

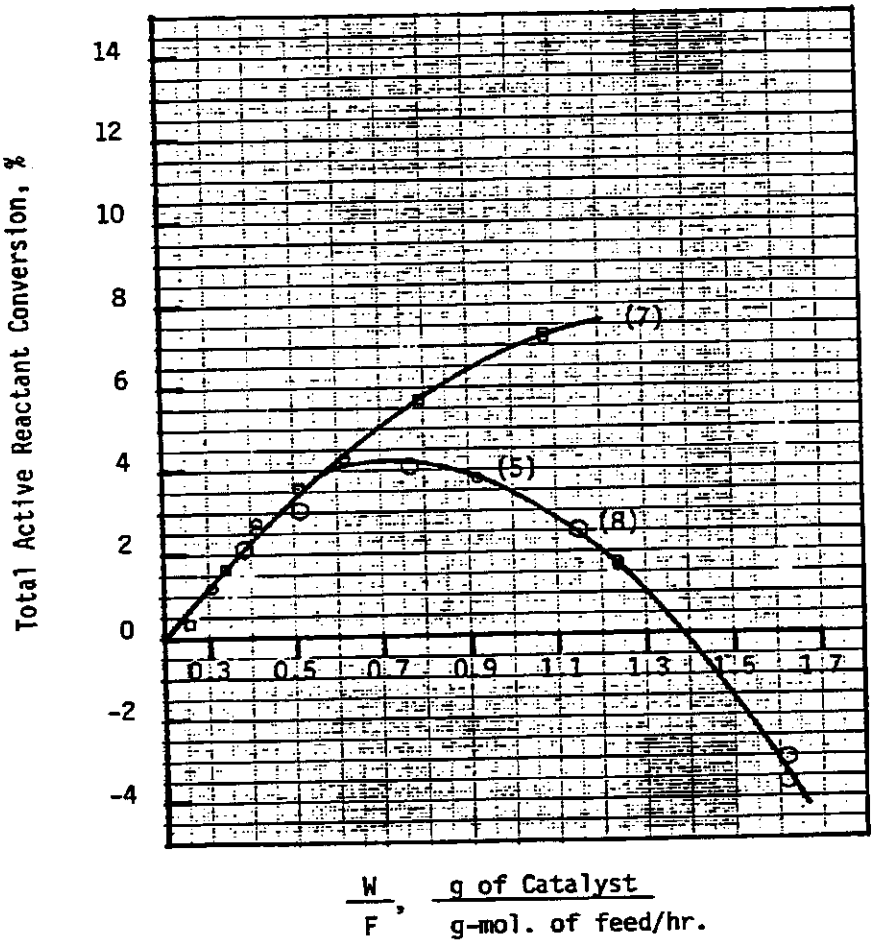

Figure 5.5. External Diffusion Study.

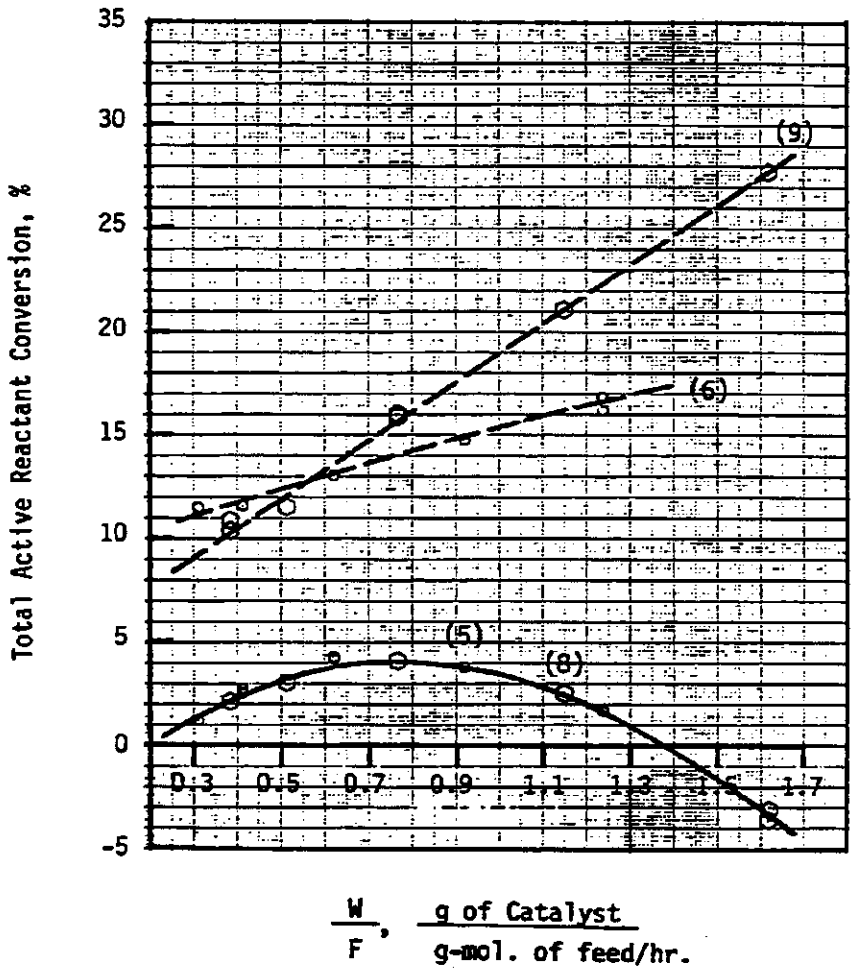

Figure 5.6. Internal Diffusion Study.

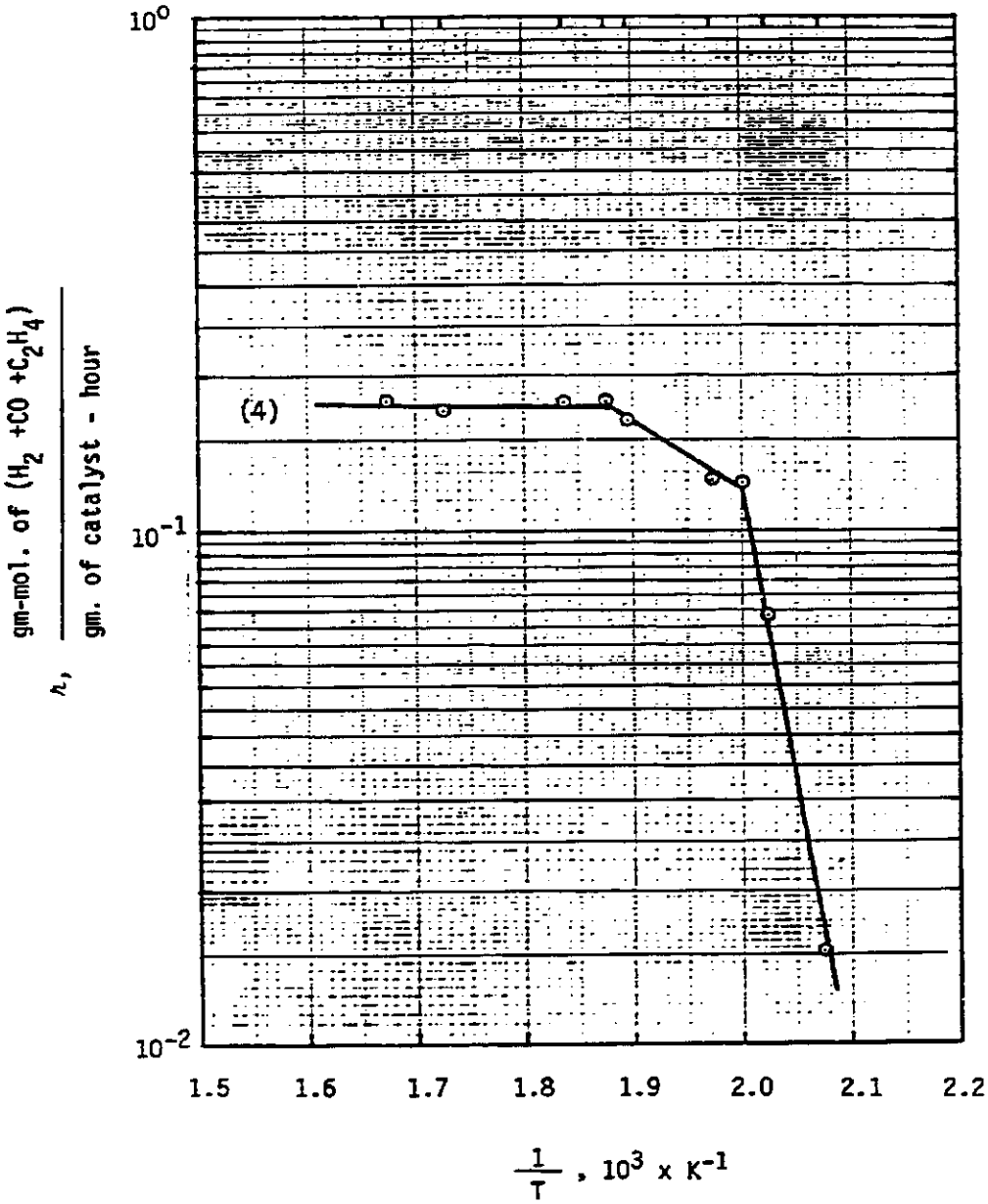

Figure 5.7. Temperature Study.

be 93.86 kJ/mol.

Theoretical criteria for negligible diffusion and temperature gradients inside a pore of the catalyst were also estimated in Appendix B and both were satisfied. The implementation of the theoretical criteria to justify the kinetic experiments, however, must proceed with caution and should always be used only as a supplement to the experimental justification.

V-4. Kinetic Experiments and Models.

Following the experimental design outlined in sections IV-4 and IV-6, the kinetic experiments were executed with four manipulating variables: operating temperature and three active reactant mass flow rates in the feed. The variations were set to cover the entire ranges allowed by the equipment. The flow rates of methane and carbon dioxide were adjusted accordingly to ensure that the WHSV is greater than the criterion of 41.4 gm/gm cat-hr determined by the justification phase of experimentation. Catalysts of 60-150 mesh (1.00 gram) from same batch were used. Total operating pressure was fixed at 140 psig. The feed conditions of all successful kinetic experiments are listed in Table 5.8.

For any type of reactor operated in a differential mode (generally less than 10% reactant conversion), the rate of reaction in terms of component i, $\mathcal{R}_i$, can be obtained directly from the experimental data of fractional conversions, ΔX_i, via the equation below [46,47,63,69,91,92,145]:

$$\mathcal{R}_i = \frac{F_i^o \Delta X_i}{W} \qquad (5.1)$$

Table 5.8. Component Flow Rates in Feed Used in Kinetic Experiments.

Run	Components, millipounds per hour.				
	H_2	CO	CO_2	CH_4	C_2H_4
1	3.36	16.0	13.7	5.6	17.6
2	3.54	48.0	41.4	0.0	26.4
4	3.54	48.0	41.4	18.0	26.4
5	4.72	64.0	55.2	24.0	35.2
6	2.36	32.0	27.6	12.0	17.6
8	4.72	64.0	55.2	24.0	35.2
9	2.38	41.2	67.4	13.7	16.6
10	1.19	20.6	67.4	13.7	8.3
12	1.79	20.6	67.4	13.7	33.1
14	1.79	82.3	67.4	13.7	33.1
15	4.76	20.6	67.4	13.7	49.7
17	1.79	20.6	67.4	13.7	8.3
18	1.79	61.7	67.4	13.7	8.3
19	1.79	82.3	67.4	13.7	8.3
20	4.76	20.6	67.4	13.7	33.1
21	4.76	61.7	67.4	13.7	33.1
24	1.19	61.7	67.4	13.7	49.7
30	1.79	20.6	67.4	13.7	49.7
31	1.79	61.7	67.4	13.7	49.7
33	2.98	51.4	67.4	13.7	29.0
34	2.98	9.7	67.4	13.7	29.0
35	2.98	93.2	67.4	13.7	29.0
39	2.98	51.4	67.4	13.7	56.8
40	2.98	51.4	67.4	13.7	20.7

where

F_i^o is the molar flow rate of component I in the feed, in gm-moles/hr, and

W is the mass of the catalyst in grams.

Large Peclet number = 334.6 and aspect ratio = 370.4 estimated in Appendix M indicates that the plug flow behavior prevails in the microreactor under the operating conditions of kinetic experiments.

The conversion data was obtained through the usual procedure for the quantitative analysis of a gas chromatograph [45,87,146,227,249]. The TCD weight response factors for active components in the gaseous product were obtained by calibration using known amounts of standards and are presented in Appendix G. Computer program GC (listed in the Appendix K) was used to perform the data analysis and reduction. Under the differential condition, almost all the kinetic experiments yielded negligible higher hydrocarbons which greatly simplified the regression fit to include only reactants and simple products. The kinetic data of reaction rate versus reaction temperature and partial pressures of active components, derived from qualified kinetic experiments, are summarized in Table 5.9.

The computer software program MODEL6B (listed in Appendix K) was coded with the incorporation of a

Table 5.9. Results of Kinetic Experiments.

Run	Rate, gm-mol / gm.cat-hr	Temp., °K	Component Partial Pressure, kPa					
			H_2	C_2H_4	CO	CO_2	CH_4	C_2H_6
N1	0.0771	489.82	383.76	150.32	375.61	68.54	83.78	4.58
N2A	0.0825	494.26	344.48	186.91	334.77	197.78	0.0	2.64
N4A1	0.0868	503.71	259.96	138.75	295.73	177.83	193.09	1.22
N5A1	0.0762	485.93	288.89	142.62	284.45	205.09	144.71	0.83
N5A2	0.1685	553.71	260.84	146.44	292.28	179.49	183.74	4.60
N5B2	0.1715	554.82	266.93	125.89	295.21	161.43	195.72	21.39
N6B	0.1807	550.37	270.95	128.64	262.31	180.10	201.42	23.18
N8B	0.2144	559.82	267.27	126.35	285.07	167.50	200.80	19.59
N9A	0.0628	496.48	213.82	100.08	271.07	311.09	167.32	3.20
N9B3	0.0975	523.71	218.00	98.94	266.73	320.88	154.94	7.09
N9B4	0.1340	549.82	211.08	91.87	262.14	323.02	163.64	14.83
N9B5	0.2007	577.59	217.03	89.69	250.76	351.71	146.47	10.92
N9B6	0.2689	605.93	207.55	87.97	242.26	370.60	146.81	11.38
N9D	0.0498	494.26	215.20	104.12	277.10	292.21	175.27	2.67
N9E	0.0411	499.82	214.53	108.48	290.61	291.75	155.10	6.11
N10	0.0435	493.15	152.83	74.41	186.25	443.99	208.61	0.50
N12	0.0513	495.93	179.97	235.28	149.89	329.88	168.45	3.09
N14	0.0193	494.82	126.81	167.72	426.12	221.53	123.78	0.62
N15	0.1048	497.04	331.81	251.99	117.34	224.66	133.24	7.54
N17	0.0432	494.26	211.82	72.41	179.09	392.71	208.23	2.33
N18	0.0126	494.26	157.28	52.50	413.26	276.16	167.37	0.0
N19	0.0113	494.26	140.71	47.27	482.38	244.54	151.68	0.0
N20	0.1295	494.26	367.10	178.22	105.73	258.47	145.05	12.01
N21	0.0670	497.04	302.49	151.86	292.99	202.92	114.87	1.45
N24	0.0293	494.26	83.34	265.33	341.72	237.87	137.22	1.10
N30	0.0590	493.71	153.59	321.95	129.05	291.82	167.22	2.96
N31	0.0382	494.26	125.82	254.07	324.17	226.46	134.87	1.19
N33A	0.0493	494.26	226.31	149.43	309.56	241.63	135.28	4.38
N33B	0.1152	527.59	231.18	128.39	283.76	256.36	146.03	20.85
N33B	0.1473	544.26	230.98	148.61	272.60	260.78	125.01	28.60
N33C	0.0567	499.82	175.85	160.56	361.63	234.41	128.97	5.17
N33C	0.1473	560.93	194.71	113.21	342.84	249.36	139.91	26.55
N34	0.1240	502.59	288.33	168.79	67.10	327.82	181.37	33.18
N35	0.0504	494.82	189.88	130.44	427.03	211.85	106.66	0.72
N39	0.0629	497.04	198.01	278.08	248.59	217.23	120.03	4.65
N40A	0.0442	494.82	237.43	118.39	313.17	244.18	136.52	16.90
N40C	0.0567	493.15	230.67	116.19	332.37	271.71	99.69	15.97

nonlinear regression routine, NLIN, of SAS Institute available through the University computing library [187], and was employed to do the data fits for the nine different kinetic models proposed in the theory chapter. Results of the fits by nonlinear regression are summarized in Tables 5.10 and 5.11. For those models that converged, the corresponding plots of predicted reaction rates versus experimentally observed ones were obtained and are presented in Figures 5.8 through 5.21. Model rejection was done by considering both the physical nature of the parameters and statistical goodness of fit.

Without adding the non-negative constraints of equilibrium constants for both adsorption and reaction, almost all models (denoted by A), except the power law, predicted at least one negative value for the equilibrium adsorption constant (see Table 5.10).

However, with the non-negative constraints added, models (denoted by B) 1, 2 and 3 simply did not converge properly. Model 8 converged, but the fitness was poor. Models 4 and 4* estimated rather large values of the equilibrium adsorption constants for both ethylene and carbon monoxide, which are physically legitimate, but it does not define the controlling steps in the reaction mechanism specifically. In model 4*, the equilibrium constant for the controlling step was not treated as an

Table 5.10. Kinetic Parameters Estimated by Nonlinear Regression.

Model	Parameters								
	a	E	K	K_2	K_3	K_4	K_{34}	K_{27}	K_{28}
1A	4.77×10^{-1}	2.96×10^{4}	4.72×10^{12}	-3.70×10^{9}	0.0	0.0	---	---	---
1B	8.76×10^{7}	1.69×10^{-4}	0.0	4.27×10^{7}	1.21×10^{9}	0.0	---	---	---
2A	2.66×10^{3}	5.67×10^{4}	-2.58×10^{14}	0.0	-2.53×10^{12}	0.0	---	---	---
2B	1.80×10^{-2}	2.26×10^{4}	0.0	0.0	3.12×10^{13}	0.0	---	---	---
3A	4.77×10^{-1}	2.41×10^{4}	3.44×10^{12}	0.0	1.80×10^{-3}	-1.31×10^{9}	---	---	---
3B	7.39×10^{13}	0.0	0.0	0.0	5.11×10^{14}	1.12×10^{14}	---	---	---
4A	3.17	3.72×10^{4}	1.41×10^{10}	1.31×10^{1}	9.51×10^{3}	5.22×10^{3}	-1.58×10^{-1}	-1.85×10^{-1}	-2.16
4B	1.20×10^{3}	3.93×10^{4}	1.07×10^{10}	6.30×10^{-2}	1.39×10^{8}	6.44×10^{7}	0.0	0.0	0.0
4A*	3.17	3.72×10^{4}	---	1.31×10^{1}	9.51×10^{3}	5.22×10^{3}	-1.58×10^{-1}	-1.85×10^{-1}	-2.16
4B*	1.16×10^{3}	3.93×10^{4}	---	6.51×10^{-2}	1.45×10^{8}	6.73×10^{7}	0.0	0.0	0.0
5A	2.81×10^{10}	3.57×10^{4}	---	4.38×10^{2}	5.98×10^{2}	9.81×10^{2}	1.50×10^{2}	1.84×10^{2}	-5.06×10^{2}
5B	1.39×10^{11}	3.64×10^{4}	---	1.10×10^{3}	1.55×10^{3}	2.51×10^{3}	4.05×10^{2}	4.12×10^{2}	0.0
6A	7.87	1.65×10^{4}	8.57×10^{2}	2.38×10^{-2}	2.31×10^{-1}	0.0	-1.50×10^{-2}	-1.79×10^{-1}	-9.54×10^{-2}
6B	3.65×10^{5}	4.01×10^{4}	0.0	3.46×10^{-2}	0.0	1.24×10^{8}	0.0	0.0	0.0
7A	1.81×10^{1}	3.42×10^{4}	---	5.80×10^{-7}	4.80×10^{-7}	2.62×10^{-3}	-2.49×10^{-3}	-1.93×10^{-2}	5.59×10^{-2}
7B	2.03×10^{2}	1.08×10^{4}	---	0.0	1.56	9.23×10^{-1}	4.14	1.79	3.53
8A	-3.00×10^{4}	2.21×10^{4}	-4.64×10^{-2}	3.84×10^{6}	4.02×10^{6}	0.0	---	---	---
8B	1.18×10^{5}	8.64×10^{4}	3.56×10^{9}	1.10×10^{16}	1.20×10^{16}	1.30×10^{16}	---	---	---
9	4.94	3.88×10^{4}		$x = 0.95$	$y = -0.23$	$z = 0.22$			

Table 5.11. Statistic Summary of Kinetic Model Fits.

Model	Degree of Freedom of Regression	Sum of Squares	Mean Square	Residual of Sum of Squares	Residual of Mean Square	Iterations to converge
1A	5	0.43642245	0.08728449	0.00869852	0.00027183	131
1B	3	0.00670862	0.00223621	0.43841235	0.01289448	61
2A	5	0.37292981	0.07458596	0.07219116	0.00225597	166
2B	3	0.00284183	0.00094728	0.44227914	0.01300821	22
3A	5	0.33322433	0.06664487	0.11189664	0.00349677	93
3B	3	0.00704806	0.00234935	0.43807291	0.01288450	32
4A	8	0.44230482	0.05528810	0.00281615	0.00009711	1371
4B	8	0.44157957	0.05519745	0.00354140	0.00012212	232
4A*	8	0.44230483	0.05528810	0.00281614	0.00009711	1405
4B*	8	0.44157939	0.05519742	0.00354158	0.00012212	266
5A	8	0.44151206	0.05518901	0.00360891	0.00012445	1120
5B	8	0.44120794	0.05515099	0.00391303	0.00013493	1101
6A	14	0.47142913	0.03367351	0.90974385	0.04135199	91
6B	6	0.42912446	0.07152074	0.00919026	0.00030634	954
7A	13	0.43594308	0.03353408	0.00237164	0.00010311	3042
7B	7	0.00000079	0.00000011	0.43831393	0.01511427	7
8A	5	0.29104438	0.05820888	0.14727034	0.00475066	88
8B	2	0.34518584	0.17259292	0.09312888	0.00273908	85
9	5	0.44162019	0.08832404	0.00350078	0.00010940	11

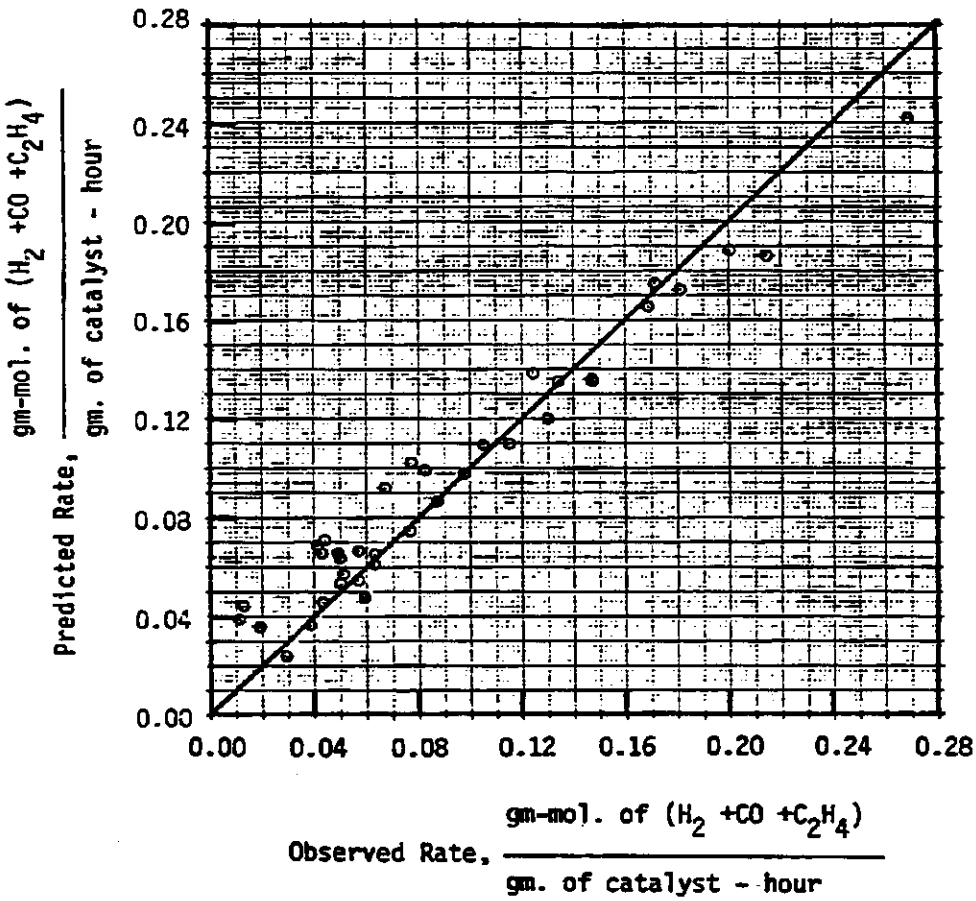

Figure 5.8. Predicted Reaction Rate vs. Observed Reaction Rate for Kinetic Model 1A.

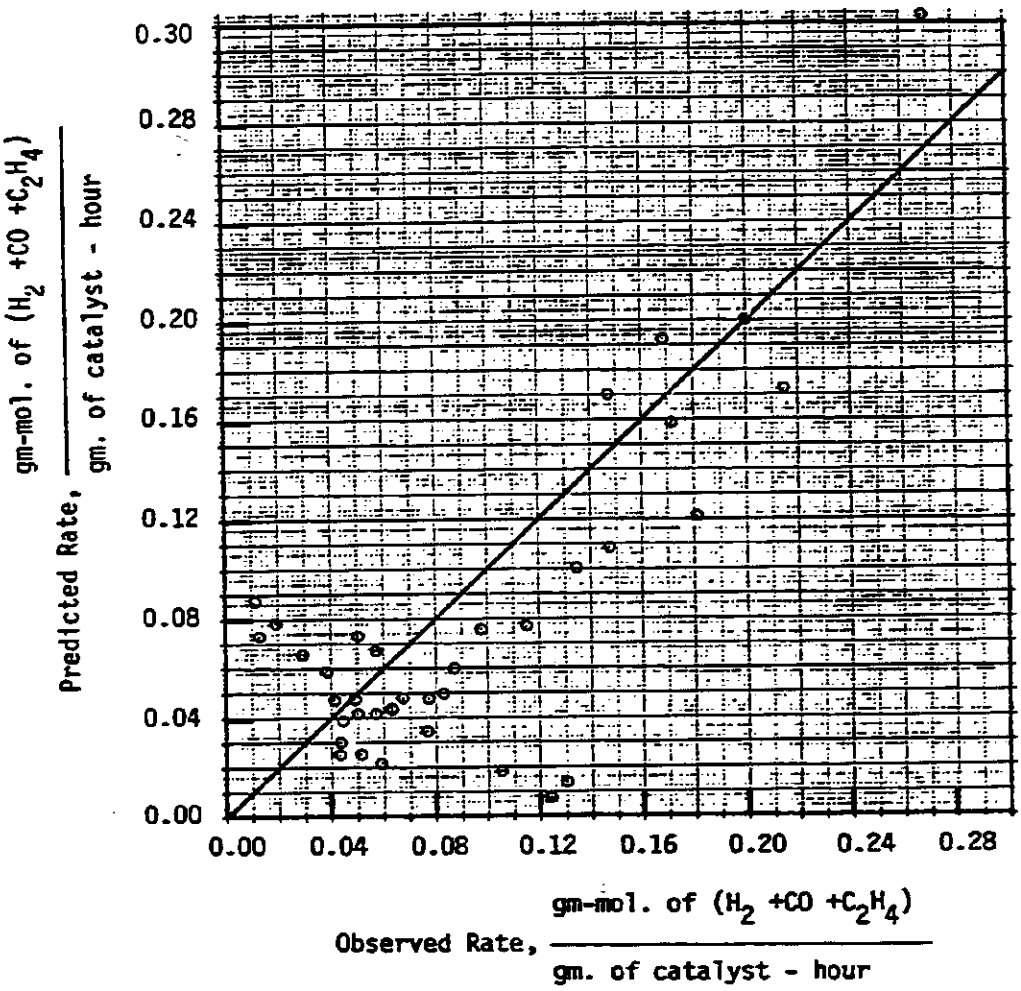

Figure 5.9. Predicted Reaction Rate vs. Observed Reaction Rate for Kinetic Model 2A.

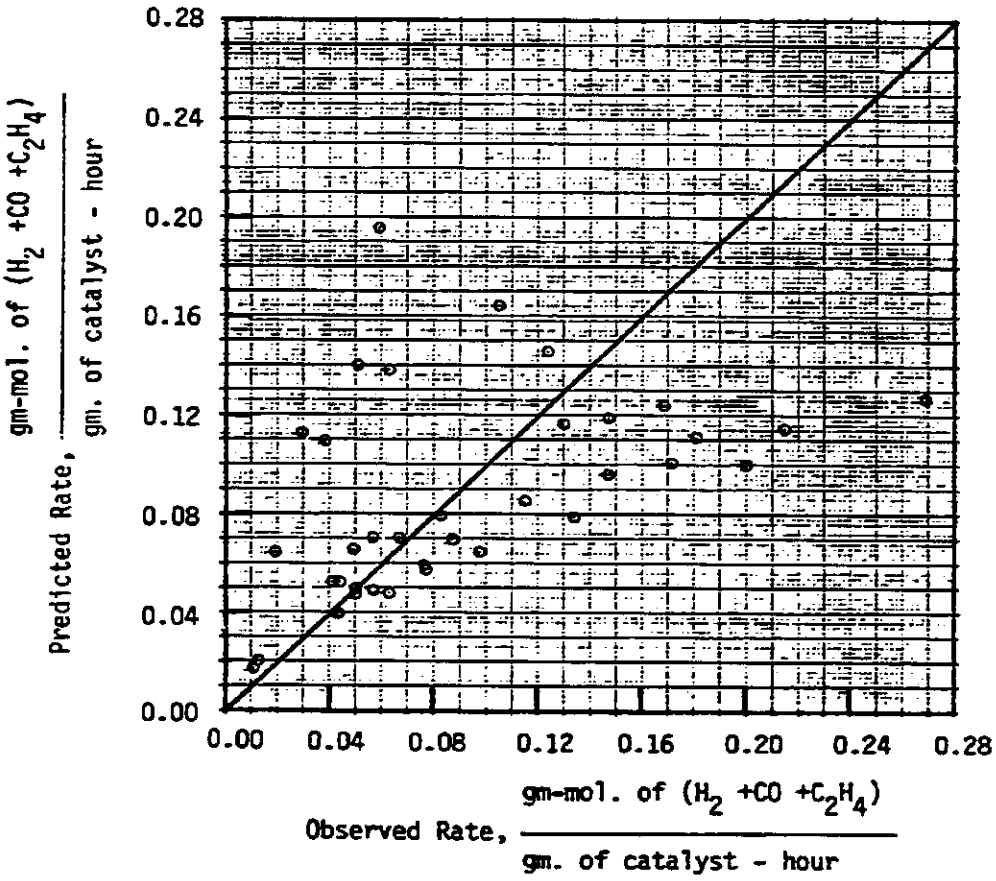

Figure 5.10. Predicted Reaction Rate vs. Observed Reaction Rate for Kinetic Model 3A.

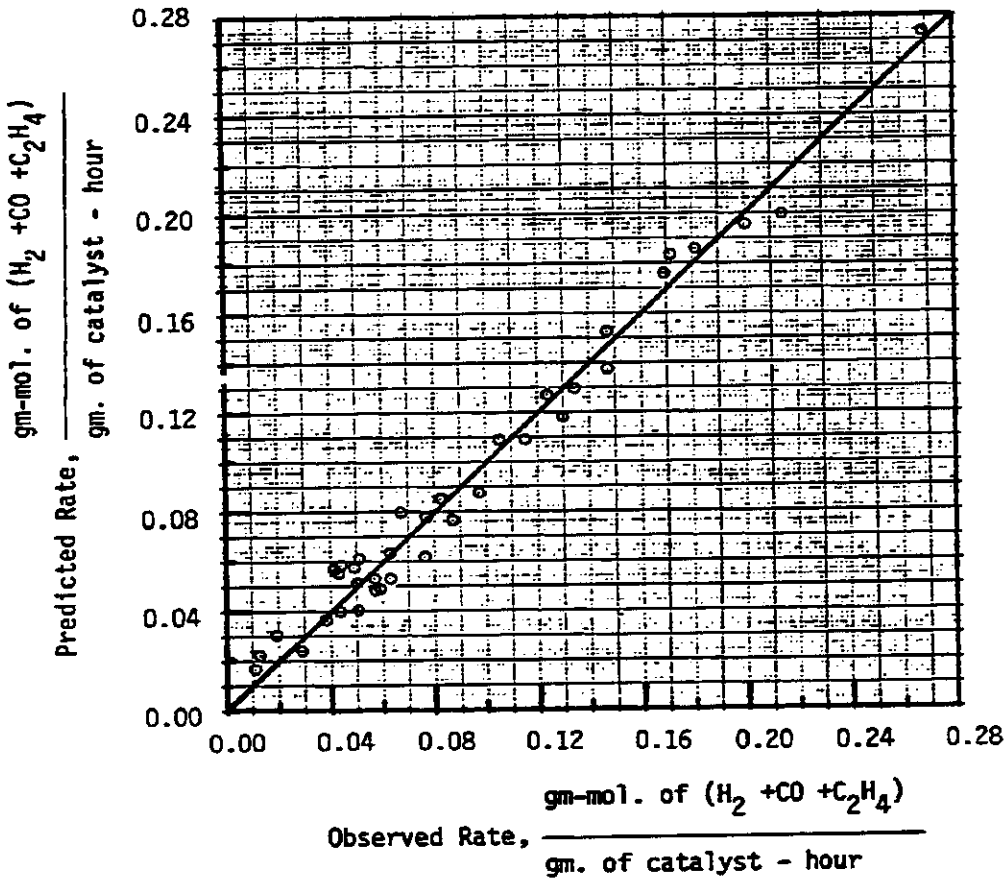

Figure 5.11. Predicted Reaction Rate vs. Observed Reaction Rate for Kinetic Model 4A.

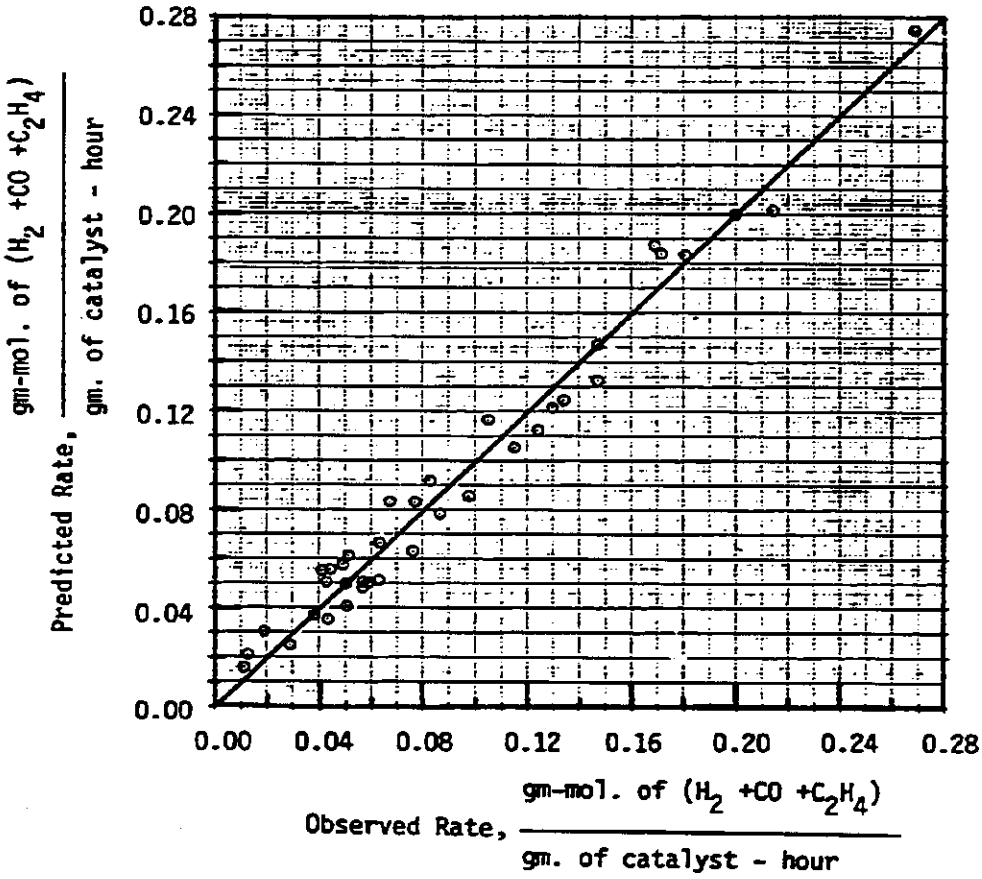

Figure 5.12. Predicted Reaction Rate vs. Observed Reaction Rate for Kinetic Model 4B.

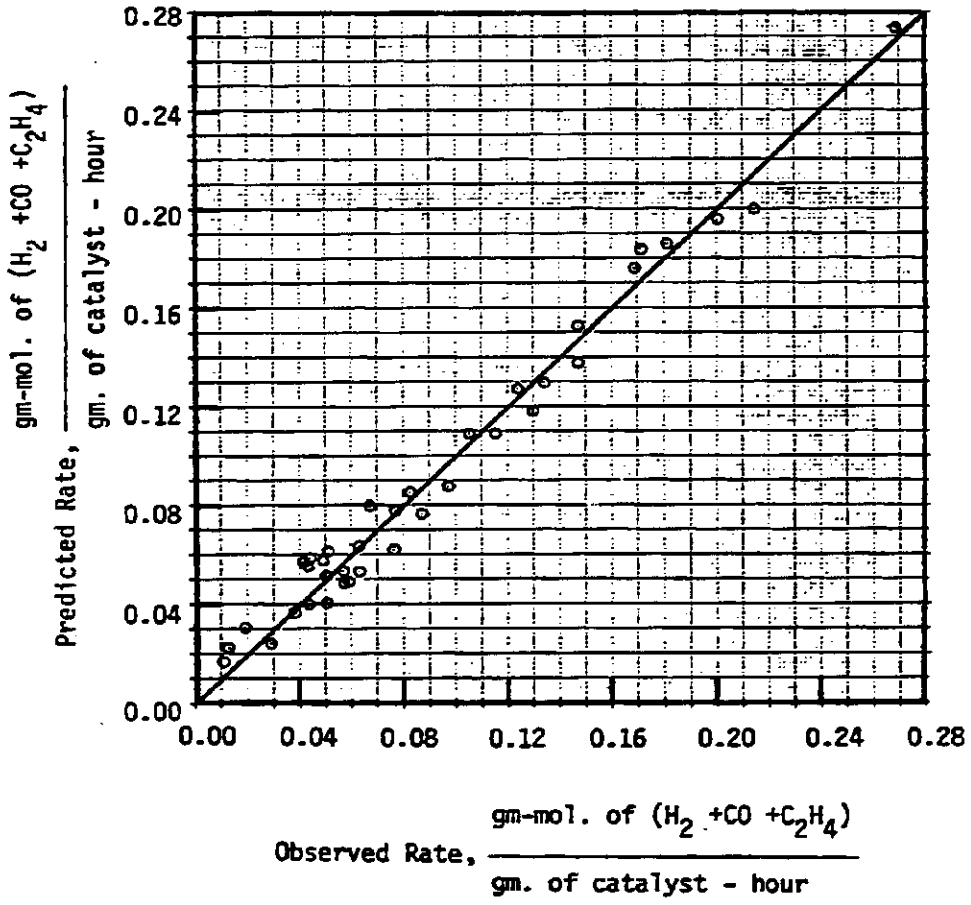

Figure 5.13. Predicted Reaction Rate vs. Observed Reaction Rate for Kinetic Model 4A*.

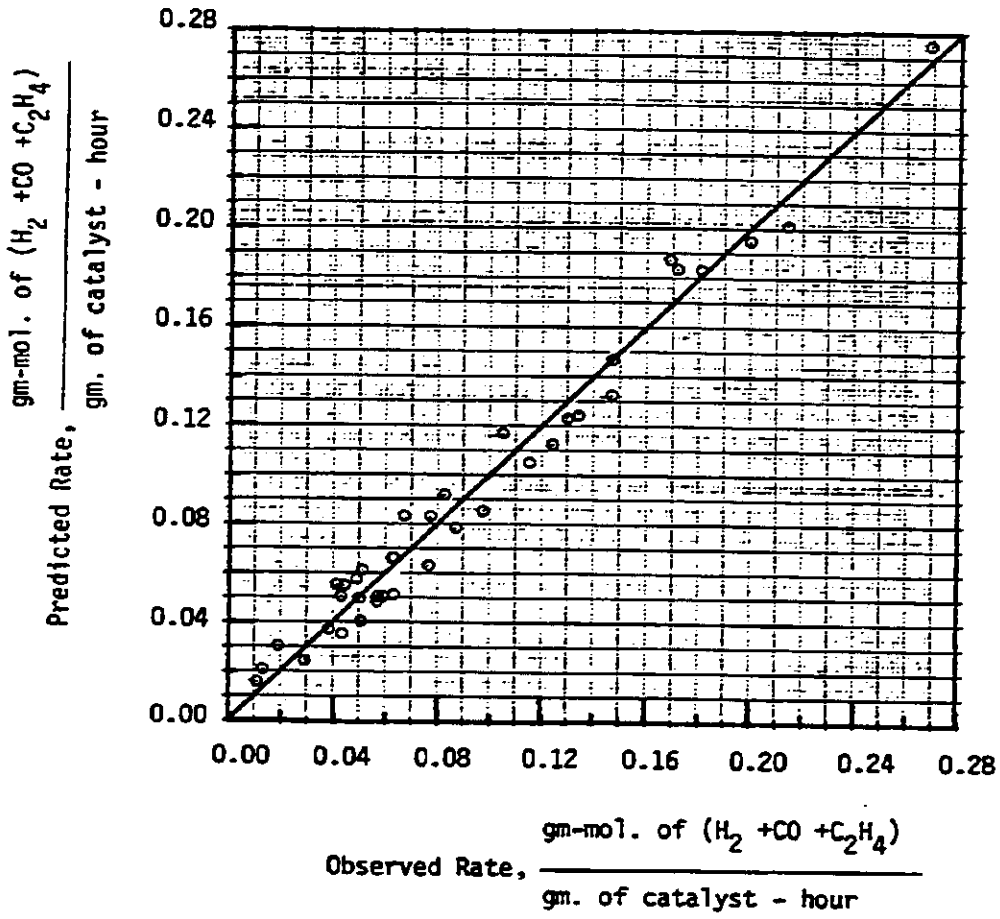

Figure 5.14. Predicted Reaction Rate vs. Observed Reaction Rate for Kinetic Model 4B*.

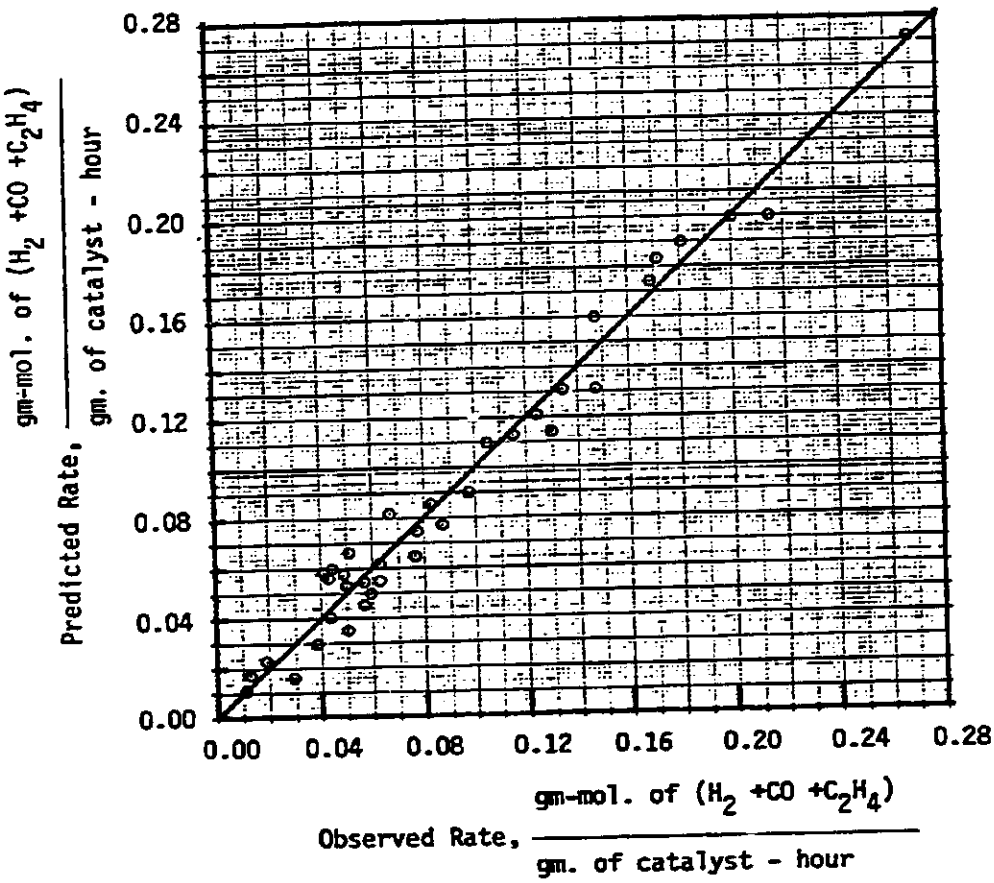

Figure 5.15. Predicted Reaction Rate vs. Observed Reaction Rate for Kinetic Model 5A -

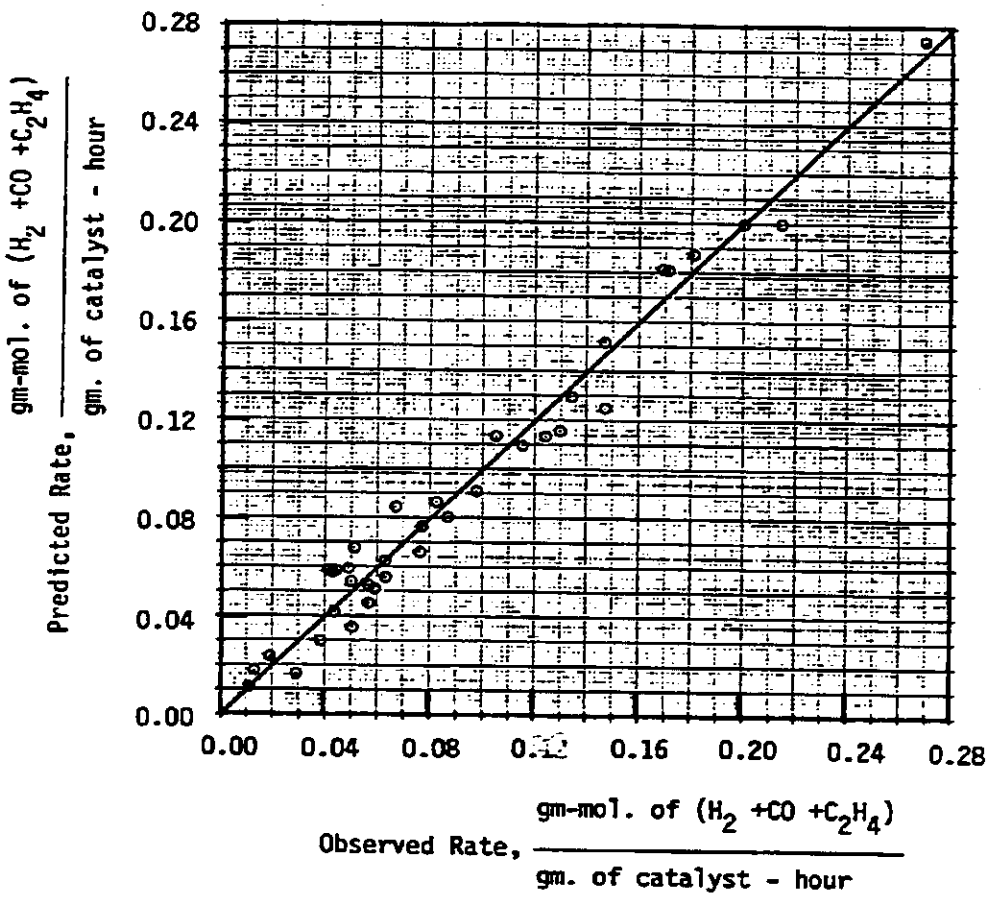

Figure 5.16. Predicted Reaction Rate vs. Observed Reaction Rate for Kinetic Model 5B.

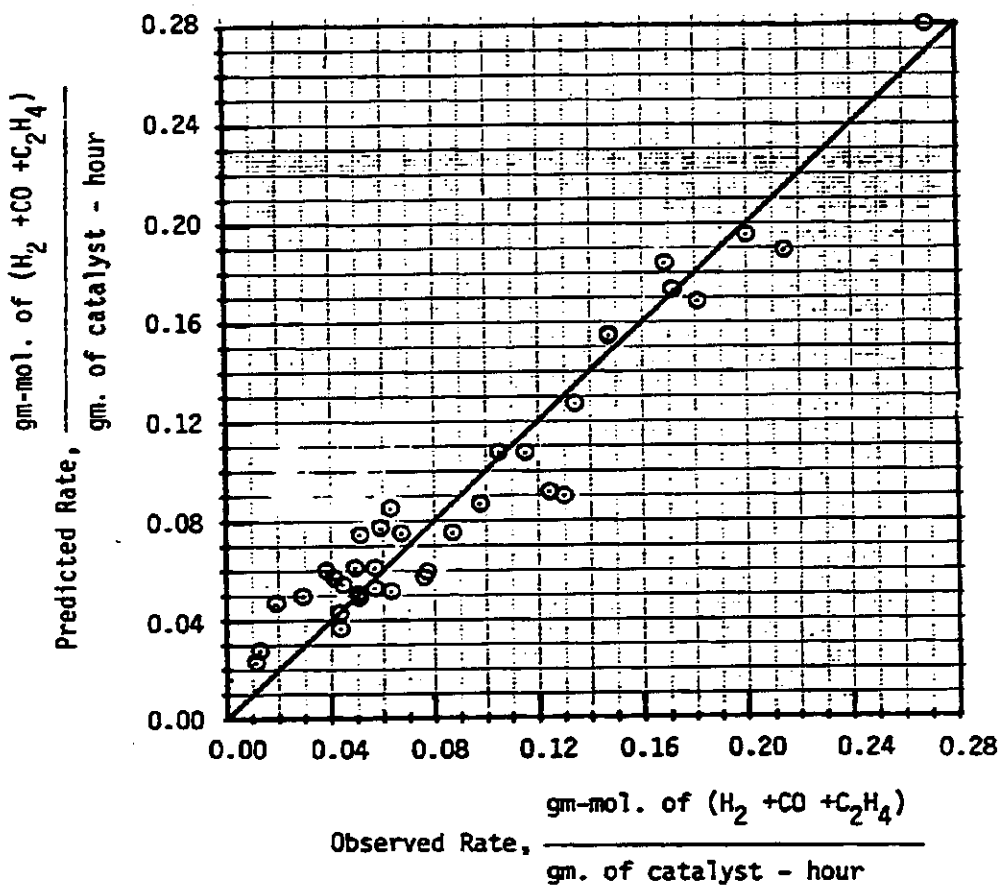

Figure 5.17. Predicted Reaction Rate vs. Observed Reaction Rate for Kinetic Model 6B.

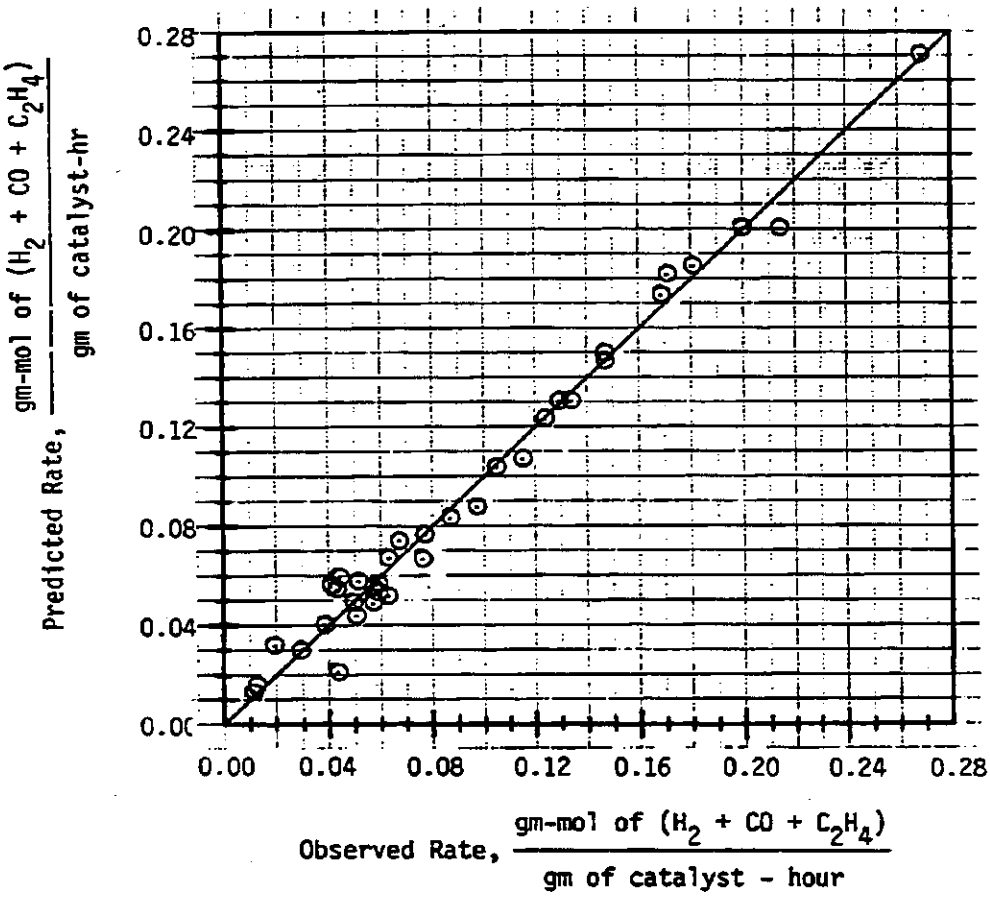

Figure 5.18. Predicted Reaction Rate vs. Observed Reaction Rate for Kinetic Model 7A.

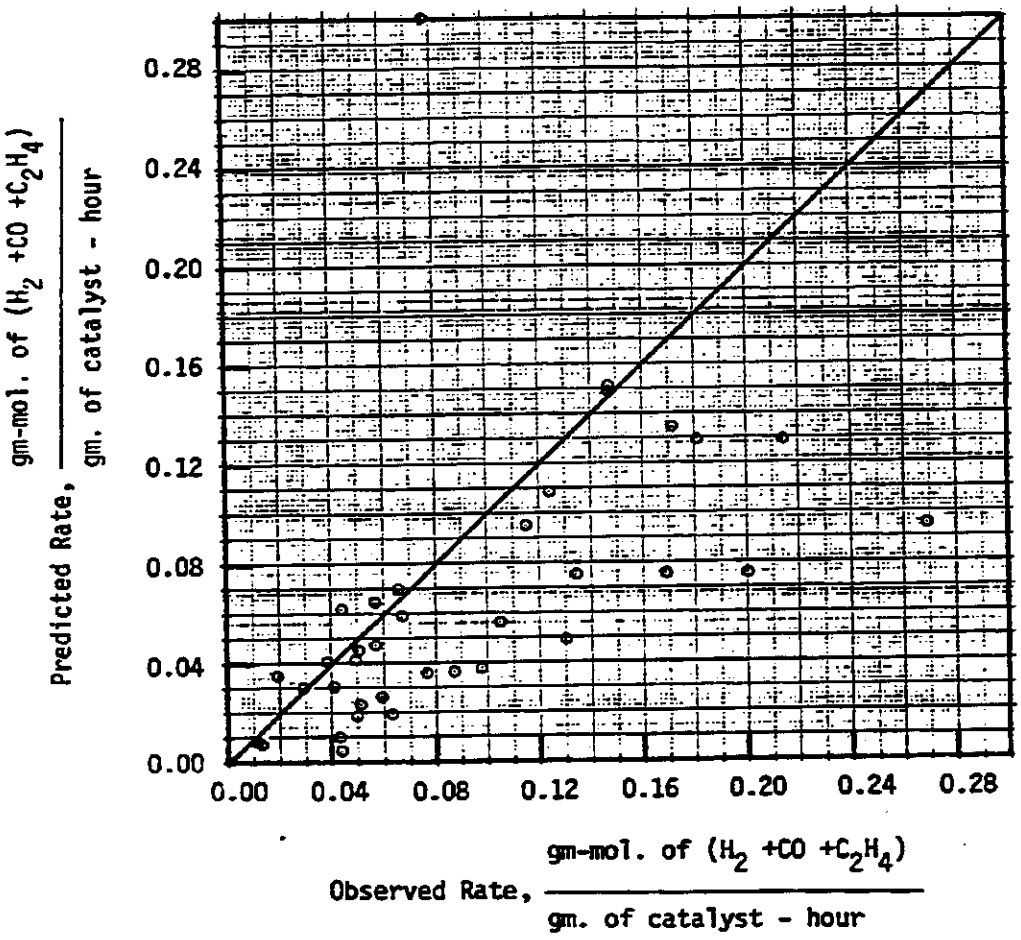

Figure 5.19. Predicted Reaction Rate vs. Observed Reaction Rate for Kinetic Model 8A.

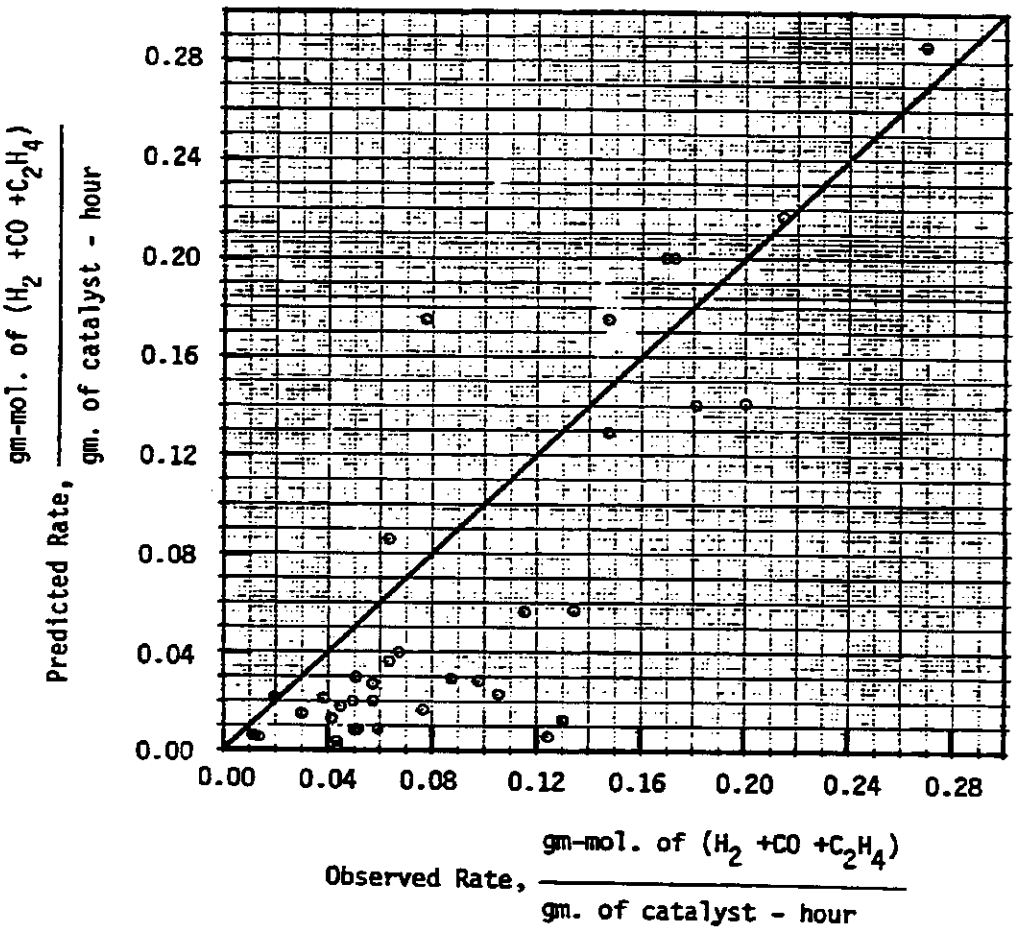

Figure 5.20. Predicted Reaction Rate vs. Observed Reaction Rate for Kinetic Model 88.

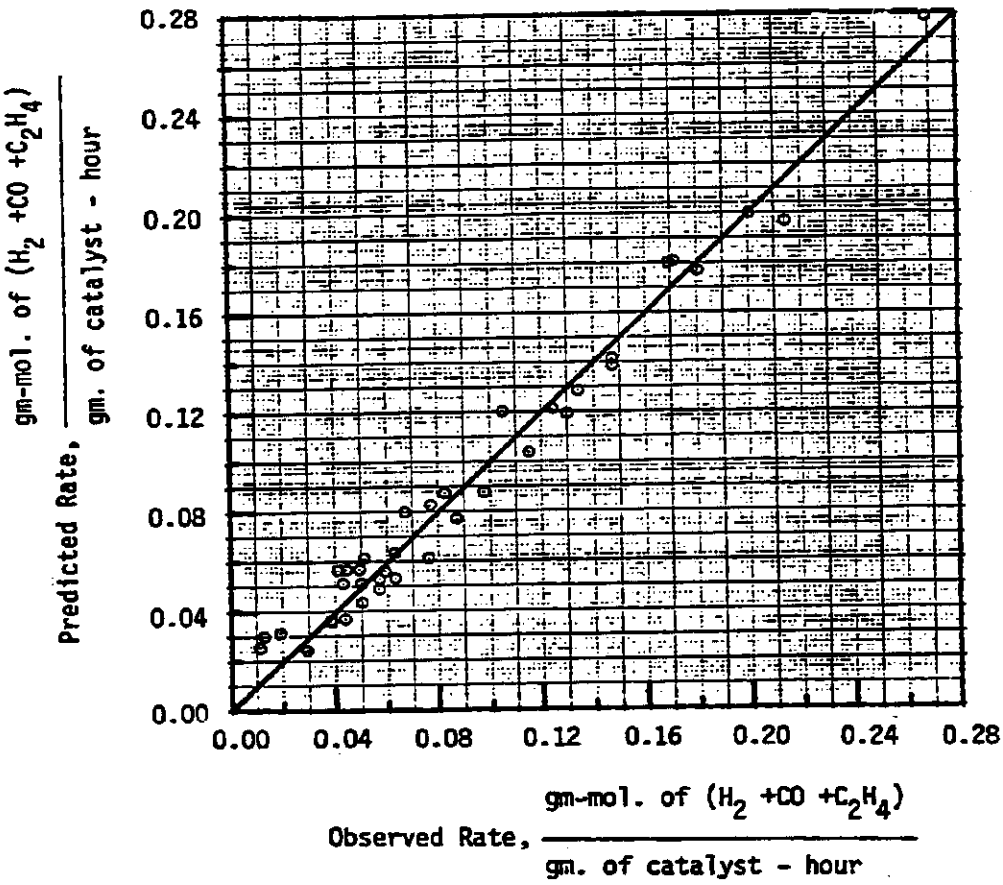

Figure 5.21. Predicted Reaction Rate vs. Observed Reaction Rate for Kinetic Model 9.

unknown parameter, instead, it was assigned a value which was obtained from the thermodynamic simulation.

Models 5 and 6 were the only two left without physical bias. Recall that both models were proposed on the basis of a surface reaction between the ethylene molecule and an adsorbed species being rate-determining. The difference between these two is that model 6 specified adsorbed hydrogen atom to be the companion reactant while model 5 only described the surface reaction in general.

It is also noted that model 9, a semi-empirical power law, is as good as theoretical models 5 and 6 as far as goodness of fit is concerned. According to Figure 5.7, the apparent activation energy, for a surface reaction controlling regime of this modified Fischer-Tropsch reaction should be 93.86 kJ/mol. However, none of values predicted by the nonlinear regression came close to this number. In fact, all the values are slightly less than half of what they should be. This means that the internal mass diffusion may play an inherent role in this synthesis. It is logical to imagine that if all the surface reactions, except the one between ethylene molecule and adsorbed hydrogen atom, occur so fast that slow diffusion of ethylene molecules through the pores of catalyst automatically governs the reaction of ethylene and hydrogen, then this in turn, controls the net rate.

V-5. Product Distribution.

Due to a variety of synthesis reactions and a vast array of hydrocarbon products that are thermodynamically possible, the carbon number distribution of total hydrocarbons for this reaction system is a complex function of catalyst and operating conditions. Products from the modified Fischer-Tropsch synthesis have been shown not to be in thermodynamic equilibrium between reactant and product species, hence valuable mechanistic information regarding the chain growth and termination can be retrieved from the selectivity data.

The main purpose of this part of the experimental work was to verify the validity of the assumption of stepwise addition of an intermediate, namely, methylene, to the growing chain proposed in the development of reaction mechanism in the theory chapter (III). This was done by checking the linearity of the plot of the logarithm of molar concentration versus the carbon number [23]. In order to be able to examine the product spectrum, the experimental conditions were relaxed from the rigid requirements for the kinetic experiments so that higher conversions could be obtained. The feed conditions for the product distribution (PD) studies are given in Table 5.12.

Table 5.12. Feed Conditions Used in Product Distribution Studies.

Study	Molar Ratio		Molar Rate (gm-mol/hr)		
	$\frac{CO}{H_2}$	$\frac{C_2H_4}{H_2}$	H_2	CO_2	CH_4
A	1.0218	0.6295	0.1282	0.0691	0.0650
B	0.9759	0.5360	0.7965	0.4267	0.5090
C	0.9474	0.5148	0.1350	0.1391	0.0650
D	0.3427	0.3765	0.7560	0.1412	0.1584
E	0.3427	0.1882	0.7560	0.1412	0.1584

The effects of reaction temperature and molar ratios of CO to H_2 and C_2H_4 to H_2 on the Schulz-Flory probability constant α, defined as the ratio of rate of chain propagation (growth) to that of chain termination (desorption), were studied. The values of α, α' and α'' (denoting straight chain paraffins, 2-monomethyl paraffins, and 1-olefins respectively), are summarized in Tables 5.13 through 5.16 and corresponding product distributions are plotted in Figures C.1 through C.36 in Appendix C.

It is observed that the chain growth of normal and monomethyl paraffins in the small carbon number range (say less than C_{20}) seems not to be heavily dependent on reaction temperature. However, for a larger carbon range, lower reaction temperatures slow down the chain growth. On the other hand, the rates of termination (desorption) are increased. Certain branched paraffins appear to grow faster than corresponding straight chains. Increasing temperature, however, does speed up the growth of 1-olefins.

As reported for conventional Fischer-Tropsch synthesis [8], water appears to be the principal component in the aqueous phase product. Normal paraffins (up to C_{35}), monomethyl paraffins and 1-olefins are the primary synthesis products. Most carbon-number distributions for

Table 5.13. Temperature Effect on Product Distribution of Study A.

Temp. (°K)	Schulz-Flory Probability Constant of Chain Growth							
	α_1	α_2	α_3	α_4	α_1'	α_2'	α_3'	α_1''
594.3	0.68	0.89	0.70	----	0.68	0.95	0.72	0.83
563.7	0.69	----	----	----	0.70	0.75	----	0.75
531.5	0.69	0.58	----	----	0.63	----	----	----
502.6	0.67	0.55	----	----	0.74	0.57	----	----
474.8	0.69	0.53	----	----	0.75	0.56	----	----

Table 5.14. Temperature Effect on Product Distribution of Study C.

Temp. (°K)	Schulz-Flory Probability Constant of Chain Growth							
	α_1	α_2	α_3	α_4	α_1'	α_2'	α_3'	α_1''
577.6	0.65	0.75	0.73	----	0.63	0.74	----	0.76
	0.67	0.83	0.54	----	0.74	0.53	----	0.72
555.4	0.69	0.53	0.79	0.82	0.72	0.58	----	----
522.0	0.74	0.64	----	----	0.72	0.69	----	0.70

Table 5.15. Effect of $\frac{CO}{H_2}$ and $\frac{C_2H_4}{H_2}$ Ratios on Product Distribution @ 555.4°K.

Study	Schulz-Flory Probability Constant of Chain Growth							
	α_1	α_2	α_3	α_4	α_1'	α_2'	α_3'	α_1''
B-1	0.66	----	----	----	0.70	----	----	----
B-2	0.72	0.84	----	----	0.76	0.82	0.91	0.78
B-3	0.72	----	----	----	0.77	0.84	----	----
B-4	0.69	0.77	----	----	0.58	0.78	----	0.77
C	0.69	0.53	0.79	0.82	0.58	----	----	----

Table 5.16. Effect of $\frac{CO}{H_2}$ and $\frac{C_2H_4}{H_2}$ Ratios on Product Distribution @ 494.3°K.

Study	Schulz-Flory Probability Constant of Chain Growth							
	α_1	α_2	α_3	α_1'	α_2'	α_3'	α_1''	α_2''
B-5	0.69	0.95	----	0.74	0.87	0.90	0.73	0.83
B-6	0.69	0.96	----	0.74	0.85	0.97	0.70	0.86
B-7	0.69	0.94	----	0.71	0.83	0.93	0.70	0.87
D	0.66	0.79	0.97	0.71	0.86	0.92	0.67	0.82
E	0.64	0.93	----	0.69	0.80	----	0.67	0.80

the total hydrocarbons on a weight basis had a minimum at C_7 and a local maximum at C_{10}. Alpha-olefins were not often observed in the product and the amount was usually quite small. Most of the carbon dioxide is believed to be generated in the secondary water-gas shift reaction [8].

The incorporation of α-olefins in the synthsis gas in the reaction does not drastically change the product spectrum of classical Fischer-Tropsch synthesis, but a shift in the product distribution toward longer chains does occur. Almost all the Schulz-Flory distribution curves obtained are straight lines, although some of them are broken into several sections. This agrees with the assumption that step addition of carbon atoms occurs one at a time. Possible reasons for the deviation from the Schulz-Flory distribution are wax deposition on the catalyst, operation in transient conditions, artifacts in sampling and effects of secondary reactions [71,126,166,167,169,170].

V-6. Experimental Error.

An example of the experimental error analysis for the base point runs has been detailed in Appendix N. The uncertainty of the reaction rate, in terms of individual reactant species, was 9.78% for ethylene, 16.54% for hydrogen, and 27.07% for carbon monoxide. The carbon monoxide rate was the worst one among the three active reactants due to severe fluctuations of the rotameter float (over 10% on the set point). The uncertainty of the reaction rate can be significantly smoothened out to 11.87% by summing the three individual reactant rates together according to the analysis.

In addition to the human error in operating the experiments, the instrumental uncertainty of the GC analysis was also examined. Typical GC peak areas of hydrogen, carbon monoxide, ethylene, carbon dioxide and methane taken from approximately 20 experiments of identical conditions (where mass flow rates of H_2, CO, C_2H_4, CO_2, and CH_4 were 2.98, 51.44, 28.97, 67.39 and 13.69 millipounds/hr respectively) were plotted in a special type of probability graph papers as shown in Figures N.1 through N.5 respectively in Appendix N. It can be seen that most data points do fall into a single straight line. This means that the distribution of random errors in the GC analysis in terms of measured peak areas is

normal.

For the same set of GC analyses, calculated TCD weight response factors of each components, however, do not quite form a straight line (see Figures N.6 through N.9 of Appendix N). In summary, two major sources of experimental errors are observed. They are: (1) the unstable flows of the feed gases, and (2) the impurities in the feed gases. The first was mainly caused by the imperfection of the rotameter manufacture. The latter led to the uncertainties in calculating the component response factors for the quantitative GC analysis.

Experimental uncertainty always exists regardless of how much care is practiced by the experimenters. Nevertheless, with good common sense and proper precaution, systematically logical investigation of experimental data can locate the major source(s) of experimental error and hence enable the experimentalist to minimize the errors in improving the accuracy of his experiments.